The Astrophysical Journal Letters, 929:L27 (11pp), 2022 April 20 https://doi.org/10.3847/2041-8213/ac6516

A Tale of Two Circularization Periods

J. J. Zanazzi
Canadian Institute for Theoretical Astrophysics, University of Toronto, 60 St. George Street, Toronto, ON M5S 3H8, Canada; jzanazzi@cita.utoronto.ca
Received 2021 December 10; revised 2022 April 5; accepted 2022 April 7; published 2022 April 26

Abstract

We reanalyze the exquisite eclipsing binary data from the Kepler and TESS missions, focusing on eccentricity measurements at short orbital periods to empirically constrain tidal circularization. We calculate a circularization period of ∼6 days due to nearly circular binaries with long orbital periods ("cold core") but find many binaries with moderate eccentricities that circularize interior to only ∼3 days ("eccentricity envelope"). We show that these features are present in previous spectroscopic surveys. We also reaffirm the statistically significant difference between the eccentricity distributions of young (<1 Gyr) and old (>3 Gyr) binaries. Our work introduces new methods that have the potential to reconcile theoretical predictions with observations to empirically constrain tidal circularization.

Unified Astronomy Thesaurus concepts: Close binary stars (254); Eclipsing binary stars (444); Tides (1702); Binary stars (154)

1. Introduction

There are two classes of tidal theories. One, championed by Zahn and collaborators, posits that tidal friction arises from the damping of the equilibrium tidal response in the turbulent convection zones (e.g., Zahn 1966, 1977, 1989; Zahn & Bouchet 1989). The main uncertainty in these theories is the efficiency of turbulent damping, especially in the so-called "fast-tide" regime. Competing theories (Goldreich & Nicholson 1977; Goodman & Oh 1997) yield friction estimates that differ by orders of magnitude (Penev et al. 2007; Ogilvie & Lesur 2012; Duguid et al. 2020a, 2020b; Vidal & Barker 2020a, 2020b).[1]

The other class of theories focuses on "dynamical" tidal responses. These consider the dissipation of tidally forced oscillations: internal gravity modes damped by radiative diffusion and turbulent convection (e.g., Zahn 1975, 1977; Goodman & Dickson 1998; Terquem et al. 1998; North & Zahn 2003) and possibly nonlinear wave-breaking (e.g., Goodman & Dickson 1998; Ogilvie & Lin 2007; Barker & Ogilvie 2010; Barker 2020); and rotationally supported inertial waves damped by viscosity (e.g., Wu 2005; Ogilvie & Lin 2007; Goodman & Lackner 2009; Lin & Ogilvie 2018, 2021). However, the generally weak tidal forcing and the transient nature of tidal resonances (Terquem et al. 1998) may conspire to make these forced oscillations unimportant. This then stimulates the recent development of the so-called "resonance locking" theories (Savonije & Papaloizou 1983, 1984; Witte & Savonije 1999, 2001; Savonije & Witte 2002; Witte & Savonije 2002; Burkart et al. 2012; Fuller & Lai 2012; Fuller 2017; Ma & Fuller 2021) whereby tidal resonances are prolonged by stellar evolution. Recent work shows resonance locking onto gravity modes efficiently circularizes binaries during the pre-main sequence, with comparatively little additional circularization during the main sequence (Zanazzi & Wu 2021).

Interestingly, while theorists are clearly excited by and invested in this problem, there are scant observational constraints. The most notable exception is the series of works by Mathieu and collaborators (Mathieu & Mazeh 1988; Latham et al. 1992; Mathieu et al. 2004; Meibom & Mathieu 2005; Meibom et al. 2006; Geller & Mathieu 2012; Geller et al. 2013; Milliman et al. 2014; Leiner et al. 2015; Nine et al. 2020; Geller et al. 2021; see also Mayor & Mermilliod 1984). Using a sample of binary orbits collected painstakingly through radial-velocity monitoring, they measured the "circularization period," or the period out to which most binaries have circular orbits, for stellar clusters at different ages. Figure 1 is the culmination of their body of works at the time (see Nine et al. 2020, for updates), where solar-type binaries younger than ∼1 Gyr are shown to be circular out to about 8 days, while this value rises to ∼15 days for those in the oldest open clusters and the halo. Given that the strength of tidal interactions drops steeply with increasing binary separation, these long circularization periods suggest that internal friction in main-sequence stars is much higher than expected by many estimates.[2] This poses a significant constraint on the tidal theories and remains an outstanding problem in astrophysics (e.g., Mazeh 2008).

Almost a decade after the pioneering work of Meibom & Mathieu (2005), there has been little independent work to examine this paper's principal conclusions, which is the goal of this paper. We are aided by results from a number of recent surveys, such as eclipsing binaries (EBs) from the Kepler and TESS photometric missions (e.g., Prša et al. 2011; Van Eylen et al. 2016; Windemuth et al. 2019; Justesen & Albrecht 2021) and radial-velocity binaries from the SDSS spectroscopic survey (Price-Whelan et al. 2017; Price-Whelan & Goodman 2018;

[1] Recently, Terquem (2021) and Terquem & Martin (2021) proposed an unsuppressed source of dissipation from turbulent convection, but see Barker & Astoul (2021) for a rebuttal.

[2] After the submission of this manuscript, the work of Barker (2022) was published. They find inertial-wave tidal dissipation circularizes binaries out to ∼8 days during the pre-main sequence and out to even longer periods during the main sequence, in agreement with Meibom & Mathieu (2005). The primary conclusions of the present publication remain unchanged, as well as the author's view on the potential importance of inertial-wave dissipation (see Section 5).

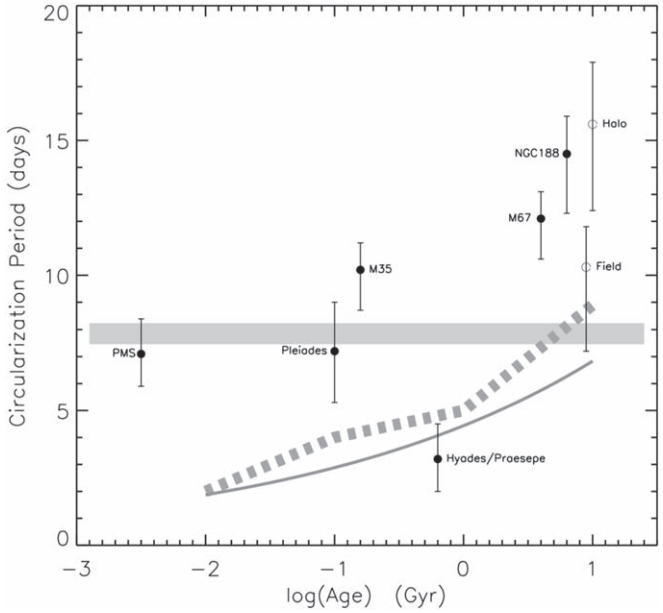

Figure 1. Figure 9 from Meibom & Mathieu (2005), reproduced with permission. Measurements of binary orbits in different clusters and environments show that the circularization period (see text for definition) rises gradually during the main sequence, from about 8 days for the pre-main-sequence populations to about 15 days for the oldest populations. The curves are predictions from various theories: The thin gray line is equilibrium tides (Zahn 1989), the thick gray line is equilibrium tides during the pre-main sequence (Zahn & Bouchet 1989), and the dotted gray line are dynamical tides including resonance locking (Witte & Savonije 1999).

Price-Whelan et al. 2020; Kounkel et al. 2021). By analyzing the EB data, we find most binaries circularize interior to ∼6 days, with a subpopulation of binaries circularizing interior to only ∼3 days, a conclusion that differs drastically from Meibom & Mathieu (2005).[3] In the following, we present and compare the data sources for our study (Section 2), our methods to constrain tidal circularization (Section 3), with our results presented in Section 4. We briefly discuss the theoretical implications of our results (Section 5) and draw our main conclusions in Section 6.

2. Data Sources

2.1. Eclipsing Binary Data

We analyze the EBs discovered by the Kepler (Borucki et al. 2010) and TESS (Ricker et al. 2015) missions. Lightcurves of EBs reveal the orbital eccentricities when both the primary and the secondary eclipses are detected (for a tutorial, see, e.g., Winn 2010; we briefly recap in Appendix A). Qualitatively, while primary and secondary transits in circular orbits occur exactly half an orbital period apart, eccentric orbits do not (unless the eccentricity vectors are fortuitously aligned with the line of sight); the durations of the two transits also encode information about the eccentricity. Hence, the precise photometric data from Kepler and TESS can reveal projected eccentricity values as minute as $\sim 10^{-3}$.

With nearly continuous photometric monitoring that spans 4 yr, Kepler discovered ∼3000 EBs with periods reaching out to ∼3 yr (Prša et al. 2011; Slawson et al. 2011; Kirk et al. 2016). These form a valuable sample for studying tidal

[3] We define a binary population as "circularized" if their eccentricities lie below a few percent.

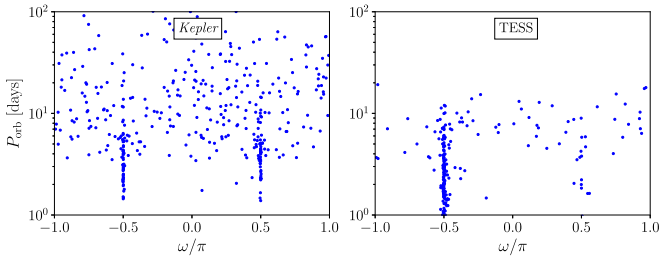

Figure 2. Calculated longitude of pericenter ω over orbital periods $P_{\rm orb}$, using the EB data from Windemuth et al. (2019) and Justesen & Albrecht (2021). The clustering around $\omega \approx \pm\pi/2$ is not real but indicates a bias due to large $e \sin\omega$ measurement errors, which tend to produce measurements with $|e \sin\omega| \gg |e \cos\omega|$. We discard $e \sin\omega$ measurements in this work.

circularization. Windemuth et al. (2019) reanalyzed Kepler lightcurves to derive orbital parameters ($P_{\rm orb}$, $e\cos\omega$ and $e\sin\omega$, where ω is the longitude of pericenter) for 728 systems. They then inferred stellar effective temperatures, radii, and masses using Gaia data and stellar isochrones. We remove the 35 systems identified by Windemuth et al. (2019) as showing transit timing variations (likely due to a tertiary companion), as well as 48 binaries that are very tight and exhibit large ellipsoidal variations (ones with morphology parameters >0.5). Neither cut impacts our study significantly.

Compared to the Kepler mission, the TESS mission has a larger field of view but a shorter monitoring duration. Justesen & Albrecht (2021) extracted ∼1000 EBs with periods extending up to 20 days. Other than the orbital parameters, they also inferred stellar parameters (stellar radii and effective temperatures, but not masses) by combining TESS folded lightcurves with the binary component spectral energy distributions, the latter obtained by combining broadband photometry with Gaia DR2 parallaxes. For our study, we append this sample to the above Kepler sample.

As we are mostly interested in the tidal dynamics of FGK stars, we retain only systems with primary masses within the range $0.8\,M_\odot \leqslant M_\star \leqslant 1.4\,M_\odot$ for the Kepler sample and effective temperatures within $4500\,{\rm K} \leqslant T_{\rm eff} \leqslant 7000\,{\rm K}$ for the TESS sample. We are left with a total of 524 EBs with $P_{\rm orb}$ values between 1 and 100 days.

In our analysis, we will only use the measured $e\cos\omega$ values but discard those for $e\sin\omega$. The former are determined by centroiding the primary and secondary transits, which can reach supreme precision. The error margin on $e\cos\omega$ is on the order of 5×10^{-4} (D. K. Windemuth 2021, private communications; Justesen & Albrecht 2021), affording us useful information on the eccentricity over several decades. In contrast, the values of $e\sin\omega$ are determined by measuring the relative widths of the transits and suffer from much larger uncertainties. For nearly circular orbits, one often measures $|e\sin\omega| \gg |e\cos\omega|$. This is indeed seen in the data (Figure 2), where the inferred ω values have an unnatural clustering round $\omega = \pm\pi/2$, a problem also pointed out by Van Eylen et al. (2016) and Justesen & Albrecht (2021).

2.2. Comparison to Spectroscopic Binary Studies

The biggest advantage of using EBs to probe tidal circularization is their precision. The Kepler/TESS photometry can measure projected eccentricity values down to $\sim 10^{-3}$. In contrast, spectroscopic binary measurements can rarely

measure eccentricities lower than a few percent (e.g., Meibom & Mathieu 2005; Triaud et al. 2017; Price-Whelan et al. 2020).

Both this work and Meibom & Mathieu (2005) use a few hundred binaries with orbital periods between 1 and 100 days, but the methods we use to analyze these samples differ. In this study, we collectively analyze the eccentricity measurements of ∼500 EBs. Meibom & Mathieu (2005) analyzed ∼200 binaries, split into seven coeval samples derived from five open clusters, pre-main-sequence stars, and the Galactic halo. They also include a sample of binaries in the Galactic field.

A deficiency of our work is a lack of reliable age estimates for our sample. Windemuth et al. (2019) provided estimates for the stellar ages, but caution that these are likely unreliable. We believe this is indeed the case—if stellar ages were drawn from a uniform distribution with a constant star formation rate over 10 Gyr, one expects no more than ∼1% of stars in the Kepler sample to have ages younger than $\sim 10^8$ yr, but ∼25% of the binaries in the Windemuth et al. (2019) catalog do so. In this work, we discard their age information. In comparison, because the binaries in Meibom & Mathieu (2005) belonged to open clusters, the age constraints on each coeval sample were exquisite.

Our study examines primaries with masses between 0.8 and 1.4 $M_\odot$ (or effective temperatures between 4500 and 7000 K), which includes some high-mass stars with radiative envelopes and convective cores (as opposed to solar-type stars with convective envelopes and radiative cores), to maintain a large sample size. Spectroscopic studies have had either more homogeneous samples of solar-like stars (e.g., Geller et al. 2021) or acknowledged when more massive stars were included (e.g., Nine et al. 2020).

3. Circularization Diagnostics

At sufficiently short orbital periods $P_{\rm orb}$, tidal dissipation circularizes the orbits of eccentric binaries. A key prediction from tidal theories is the orbital period that separates binaries with yet to be circularized orbits from binaries with nearly circular orbits. The leading empirical measure for tidal circularization was developed by Meibom & Mathieu (2005), who used binary eccentricity data to determine the longest period at which binaries circularized their orbits, called the circularization period $P_{\rm circ}$. However, the circularization period is sensitive to circular binaries with long orbital periods (see, e.g., Figure 10 of Geller et al. 2021). Motivated by this, we introduce a complementary metric that measures the period when only the most-eccentric binaries circularize their orbits, which we call the envelope period $P_{\rm env}$. Here, we review how to calculate the circularization period $P_{\rm circ}$ and introduce our new measure for tidal circularization, the envelope period $P_{\rm env}$.

We start off with the following functional form for the eccentricities:

$$e(P_{\rm orb}) = \begin{cases} 0 & P_{\rm orb} \leqslant P' \\ \alpha\left[1 - \left(\dfrac{P'}{P_{\rm orb}}\right)^{\beta}\right] & P_{\rm orb} > P', \end{cases} \tag{1}$$

with three free parameters P', α, and β. This form differs slightly from that in Meibom & Mathieu (2005): $\alpha(1 - \exp[0.14(P' - P_{\rm orb})])$. Our form is slightly simpler and returns similar values for P' when applied to the samples used in Meibom & Mathieu (2005). We then follow two different ways to characterize the circularization period. For the first, we follow Meibom & Mathieu (2005) to minimize the metric

$$\chi^2 = \sum_i [e(P_i) - y_i]^2, \tag{2}$$

where the summation is over all binary systems. The measurements $y_i = e_i \cos\omega_i$ for the projected eccentricities of EBs, or $y_i = e_i$ for the full eccentricities of spectroscopic binaries, with $_{Pi}$ denoting the binary's measured orbital period. This is similar to the procedure in Meibom & Mathieu (2005) (we ignore measurement errors[4]), and we denote the circularization period thus obtained as $P' = P_{\rm circ}$.

However, when the short-period–eccentricity distribution is complex, we find that $P_{\rm circ}$ alone does not adequately describe all the distribution's properties. The original $P_{\rm circ}$ fits for where most binaries become circular, but it does a poor job of describing the shortest-period eccentric binaries. Because these eccentric binaries can tell us additional information about the circularization history (such as the circularization of young versus old binaries; see below), we devise a metric that emphasizes the upper envelope of the eccentricity distribution. To do this, we first separate binaries into 20 logarithmic period bins and pick the most eccentric binary within the bin. We then fit Equation (2) to these maximum eccentricities at binned orbital periods. We denote the best fit P' thus obtained as $P_{\rm env}$ for the "envelope period" of the distribution.

Uncertainties on the circularization and envelope periods are typically dominated by the finite sizes of our samples, as opposed to eccentricity measurement errors. To estimate these, we calculate the errors on the circularization and envelope periods via bootstrapping, randomly reselecting N_b binaries from the original sample (some measurements can be counted more than once, while others are left out), and fit the data for the circularization $P_{\rm circ}$ and envelope $P_{\rm env}$ periods. We repeat this process N_s times and calculate the median and 1σ uncertainties from the distribution of fitted values.

To demonstrate the difference between $P_{\rm circ}$ and $P_{\rm env}$, we perform a suite of tidal simulations for binaries with ages between 1 and 10 Gyr, synthetically observing a subset of N_b EBs (see Appendix B for details). Figure 3 displays the results of this calculation, varying N_b and how strongly the tidal dissipation depends on binary separation through the parameter η:

$$\frac{1}{t_{\rm circ}} = \frac{1}{e}\frac{{\rm d}e}{{\rm d}t} \propto P_{\rm orb}^{-\eta}. \tag{3}$$

We note that these calculations also take into account inward migration while the binary population circularizes. For a small binary sample size ($N_b \lesssim 50$), there are too few binaries to reveal the complex eccentricity distribution created by the binary age range, with $P_{\rm circ}$ and $P_{\rm env}$ being statistically indistinguishable. As N_b rises, not only do the errors on the measurements of $P_{\rm circ}$ and $P_{\rm env}$ decrease, but the median $P_{\rm env}$ value decreases as well because more young binaries with high eccentricities are "observed" in the sample. In addition, the median $P_{\rm circ}$ also becomes smaller as N_b increases but does not

[4] Our methods for empirically constraining tidal circularization are designed for EBs whose measurement errors are negligible. Although measurement errors are available for the spectroscopic binary sample, we ignore them so we can use the same statistical methods.

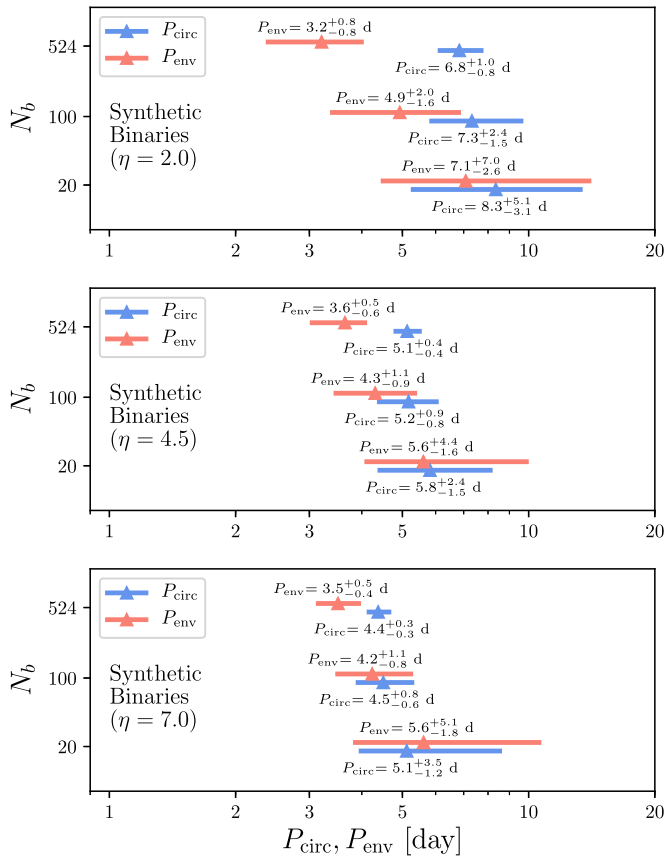

Figure 3. Circularization $P_{\rm circ}$ (blue) and envelope $P_{\rm env}$ (orange) periods for the synthetically observed binaries, varying the number of binaries N_b drawn from the tidally circularized population, for the values of η (Equation (3)) indicated. Triangles and lines denote the median and 1σ uncertainty values (also displayed above/below lines). See Appendix B for details.

come close to the sharp dependence of $P_{\rm env}$ on N_b. We see for a distribution of binaries with different ages that $P_{\rm env}$ emerges as a way to measure the circularization of young binaries for large samples ($N_b \gtrsim 100$).

In the next section, we will calculate $P_{\rm circ}$ and $P_{\rm env}$ for the Kepler/TESS eclipsing field binaries, as well as the young and old open cluster spectroscopic binaries from Meibom & Mathieu (2005).

4. Empirical Constraints on Tidal Circularization

4.1. Eclipsing Binaries

Here, we use the Kepler/TESS EB sample to calculate the circularization and envelope periods to empirically constrain tidal circularization. Figure 4 displays the EB data in the period–eccentricity (actually $|e\cos\omega|$) space. We present them in both linear and logarithmic eccentricities. The latter information is unique to EBs and a testament to the power of transit missions. Before analyzing this data using the methods described in Section 3, we notice two qualitative features of the data. The first is the presence of moderately eccentric ($|e\cos\omega| \gtrsim 0.1$) binaries, which only circularize interior to orbital periods of $\sim$3 days, a feature we label as the "eccentricity envelope." The second is the abundance of nearly circular ($|e\cos\omega| \lesssim 0.03$) binaries, which extend to orbital periods of $\sim$10 days, which we call the "cold core," borrowing terminology used to describe dynamically hot and cold Kuiper Belt objects (e.g., Morbidelli et al. 2008). Despite the density of binaries appearing roughly uniform in $\log P_{\rm orb}$, we distinguish these features in the $e-P_{\rm orb}$ diagram because they place unique constraints on theories of tidal dissipation (see Section 5 for discussion).

As is clear from Figure 4, the observed population harbors a cold core of circular binaries that extend well beyond the eccentricity envelope. These binaries produce larger values for $P_{\rm circ}$ than found for $P_{\rm env}$ because $P_{\rm circ}$ is sensitive to long-period circular orbits. Calculating the circularization period, we find $P_{\rm circ} = 6.2^{+1.4}_{-0.8}$ days, but the data clearly show many eccentric binaries with $P_{\rm orb}$ values shorter than $P_{\rm circ}$ (also see Kjurkchieva et al. 2017; Triaud et al. 2017). Calculating the envelope period instead, we find the much shorter value of $P_{\rm env} = 3.2^{+0.6}_{-0.3}$ days.

This exercise reveals that $P_{\rm env}$ lies significantly below the $P_{\rm circ}$ values calculated by Meibom & Mathieu (2005). We argue the most important reason the eccentricity envelope was missed is the difference in sample sizes. While we use 524 binaries to collectively determine a circularization period, Meibom & Mathieu (2005) determined one such period for each cluster, based on a couple of dozen binaries, and the number of binaries that provide the most stringent constraints (orbital periods from a few to a few tens of days) is even smaller. To demonstrate the impact this casts on the results, we randomly draw N_b binaries from the 524 EB sample and redetermine the circularization period. We only include EBs with periods shorter than 100 days as they provide the best constraints on the circularization period.

The top panel of Figure 5 presents results from such an exercise. With $N_b = 20$ (similar to the sample size of spectroscopic binaries in a given cluster of Meibom & Mathieu 2005, $\sim$10–50), we find a wide range of results, with $P_{\rm circ} = 8.4^{+3.5}_{-2.4}$ days, encompassing all cluster results in Figure 1 to within 2σ (see also vertical lines). This range contracts as N_b rises. As with our tidal simulations (see Figure 3), the median values for $P_{\rm env}$ (and $P_{\rm circ}$ to a lesser extent) decrease, indicating a bias for longer envelope (and circularization) periods when the sample size is small.

However, although our eccentricity measurements are more precise than those used in the Meibom & Mathieu (2005) study, we cannot date the binary ages, and our sample may include more massive hosts (see Section 2.2 for a discussion). Indeed, comparing the young (age $<$1 Gyr) and old (age $>$3 Gyr) cluster $P_{\rm circ}$ measurements from Meibom & Mathieu (2005), older binaries still have longer $P_{\rm circ}$ values compared to young ones (Figure 4). In the next subsection, we reanalyze the Meibom & Mathieu (2005) data set to reinvestigate the statistical significance of the longer $P_{\rm circ}$ values for older binaries.

4.2. Spectroscopic Binaries

In the previous subsection, we showed that a large ($N_b \gtrsim 100$) data set of binary eccentricities reveals structure not present in smaller ($N_b \lesssim 50$) subsamples. To test if the "eccentricity envelope" and "cold core" found in the Kepler/TESS data evolve with age, we examine the young ($<$1 Gyr) and old ($>$3 Gyr) binaries from the Meibom & Mathieu (2005) data set collectively (not separating binaries by cluster, Figure 6), adding into consideration new binaries from Leiner et al. (2015) for M35, and from Geller et al. (2021) for M67 (see top panel of Figure 6). The data look qualitatively very

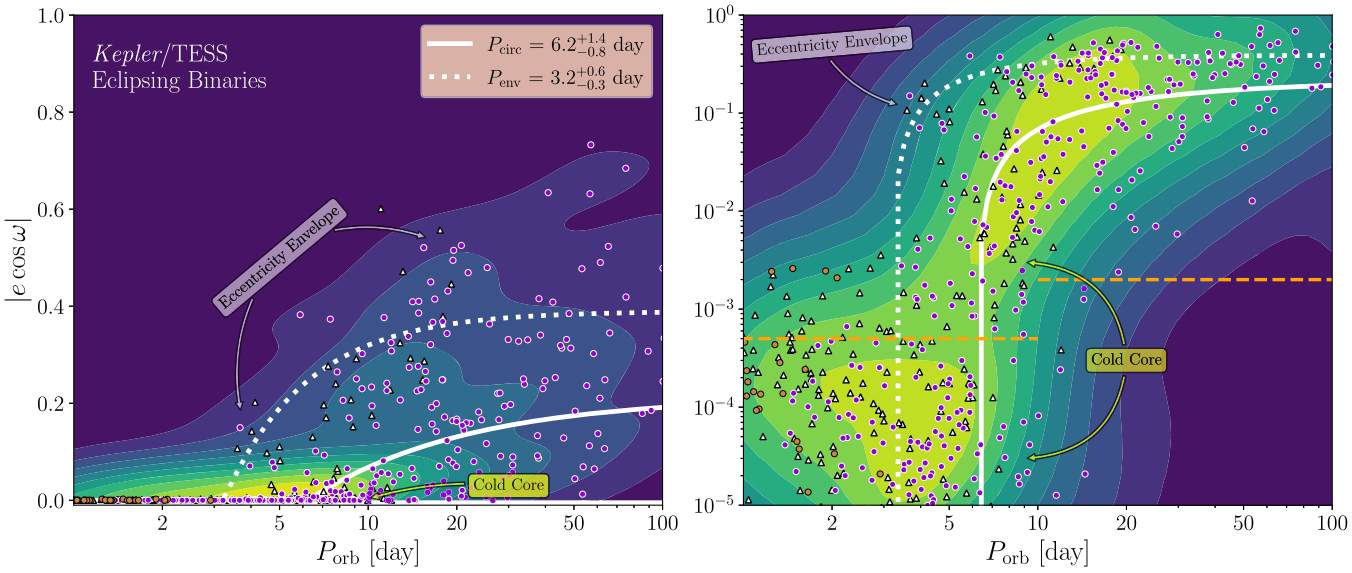

Figure 4. Eccentricity data from Kepler (purple points) and TESS (white triangles), with contours denoting smoothed kernel density estimates of the eccentricity measurements. The dashed orange line denotes typical errors in $|e\cos\omega|$ measurements in the Kepler/TESS data set, while light-brown points denote removed binaries with morph > 0.5 (see text for discussion). White solid and dotted lines denote fits for the circularization ($P_{\rm circ}$) and envelope ($P_{\rm env}$) periods. We take $N_s = 3000$, with the other parameter fits being $\alpha_{\rm circ} = 0.21^{+0.79}_{-0.06}$, $\beta_{\rm circ} = 0.8^{+1.2}_{-0.7}$, $\alpha_{\rm env} = 0.39^{+0.06}_{-0.05}$, and $\beta_{\rm env} = 1.5^{+1.0}_{-0.6}$. See text for discussion of the "eccentricity envelope" and "cold core" labels.

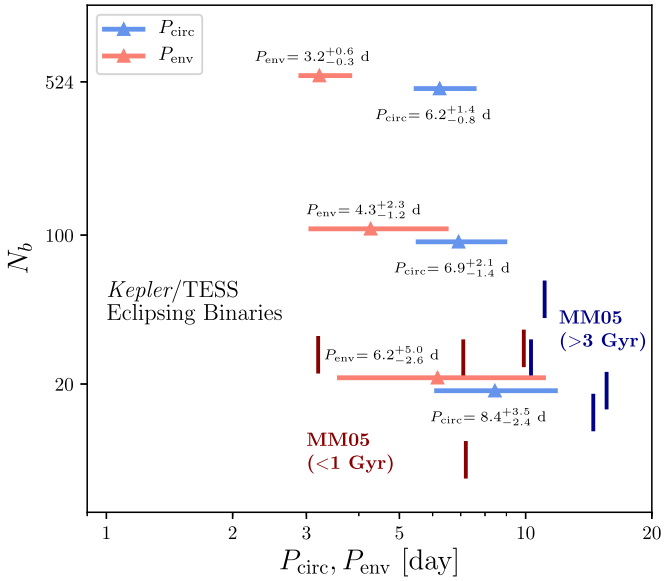

Figure 5. Circularization $P_{\rm circ}$ (blue) and envelope $P_{\rm env}$ (orange) periods for the Kepler/TESS EBs, varying the number of binaries N_b drawn from the data set, with triangles and lines denoting the median and 1σ uncertainty values (also displayed above/below lines). Young (<1 Gyr; dark blue) and old (>3 Gyr; dark red) Meibom & Mathieu (2005) circularization period measurements are shown for comparison, with N_b denoting the number of cluster measurements with orbital periods less than 100 days.

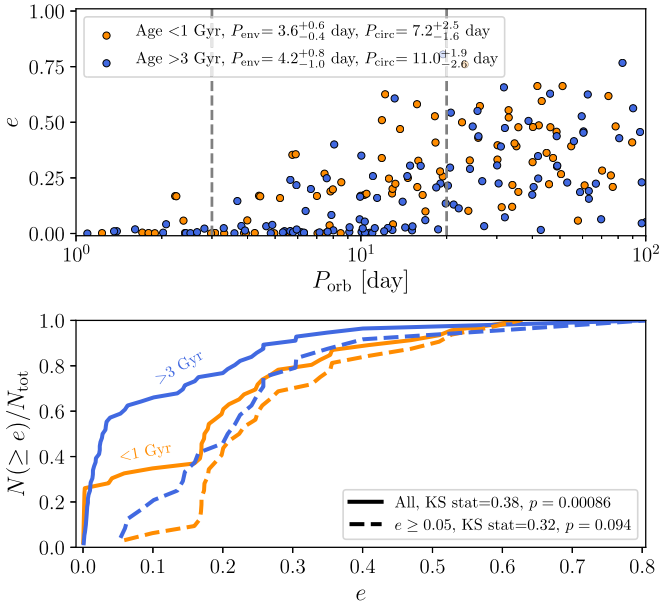

Figure 6. Top panel: young (<1 Gyr, orange) and old (>3 Gyr, blue) binaries from the Meibom & Mathieu (2005) data set (with updates in M35, Leiner et al. 2015, and M67, Geller et al. 2021). Vertical gray dashed lines delineate orbital periods of 3–20 days. Bottom panel: cumulative eccentricity distribution for the young (orange) and evolved (blue) binaries between 3 and 20 days, for no eccentricity cutoff (solid) and an eccentricity cutoff of $e > 0.05$ (dashed). The legend gives results from a two-sample KS test between the young and old binaries, showing the "eccentricity envelope" ($e > 0.05$) is consistent with no evolution with age ($p > 0.05$).

similar to our EB sample, with a clear upper envelope in eccentricity that rises with orbital period and an overdensity of nearly circular binaries out to beyond ∼10 days. In the bottom panel of Figure 6, we compare the eccentricity distributions for young and old binaries with orbital periods from 3 to 20 days, i.e., the range over which the impact of tidal dissipation is most prominent. A two-sample Kolmogorov–Smirnov test returns a probability of $p = 8.6 \times 10^{-4}$, or it is unlikely that the two distributions are drawn from the same underlying one. Moreover, the older group contains more systems that are circular.

Taken at face value, this would support the Meibom & Mathieu (2005) claim that tidal circularization operates effectively during the main sequence. However, the two populations share the same upper envelope, with $P_{\rm env} = 3.6^{+0.6}_{-0.4}$ days for the young sample and

$P_{\rm env} = 4.2^{+0.8}_{-1.0}$ days for the old ones. The two deviate from each other mostly in that the older one has a prominent cold core, with $P_{\rm circ} = 7.2^{+2.5}_{-1.6}$ days for the young and $P_{\rm circ} = 11.0^{+1.9}_{-2.6}$ days for the old. If we instead only compare binaries with $e \geqslant 0.05$, i.e., ignoring the cold cores, the Kolmogorov–Smirnov (KS) test returns a p-value of $p = 0.094$, not significant enough to reject the null hypothesis of drawing from the same distribution ($p < 0.05$). This casts some doubts on the interpretation of ongoing tidal circularization because $P_{\rm env}$ does not increase with age.

In conclusion, we find that it is hard to robustly determine the envelope period using a small sample of binaries (few tens). This explains much of the tension between our work and that of Meibom & Mathieu (2005). However, the old and young populations in their study do appear to be statistically different, and a proper understanding of these data is required to draw a robust conclusion.

5. Discussion

In this section, we briefly discuss the implications of our findings on theories of tidal circularization, and previous works that have a bearing on our results.

5.1. The Cold Core and the EBs

The presence of the cold core is puzzling. We posit three possibilities for its formation, giving three separate interpretations for the envelope ($P_{\rm env}$) and circularization ($P_{\rm circ}$) periods:

1. Disk migration and damping formed the core primordially (e.g., Kratter et al. 2010; Moe et al. 2019; Tokovinin & Moe 2020), implying $P_{\rm env}$ is the only "true" measure of tidal circularization.
2. Inertial waves preferentially synchronized then circularized stars with initially short rotation periods, so $P_{\rm env}$ and $P_{\rm circ}$ probe two separate tidal dissipation mechanisms.
3. Different $P_{\rm env}$ and $P_{\rm circ}$ values probe the circularization of binaries with different ages.

Figure 6 tentatively disfavors the third hypothesis because the seeming increase of $P_{\rm env}$ with age is not statistically secure. Reliable age and rotation period data can further illuminate the observed difference in $P_{\rm circ}$ and $P_{\rm env}$. In Section 5.3.2, we elaborate on the implications of these interpretations.

The short-period eccentric binaries probed by the envelope period may also be an abnormality, recently excited by three-body interactions (e.g., Mazeh & Shaham 1978; Fabrycky & Tremaine 2007; Naoz & Fabrycky 2014; Moe & Kratter 2018; Hamers 2019) or heartbeat pulsations (e.g., Fuller 2017; Zanazzi & Wu 2021). This would also explain why the young binaries in the Meibom & Mathieu (2005) sample have a less pronounced cold core. Here we argue that this possibility is unlikely, considering the high-precision EB data. Plotted in the logarithmic–eccentricity space (right panel of Figure 4), the EB data clearly show the "waterfall" feature, seen also in synthetic observations of EBs (see Appendix B). The eccentricities fall sharply over a narrow period range as the tidal circularization timescale drops steeply with orbital period. This strong feature of tidal dissipation is difficult to replicate through other processes.

Compared to spectroscopic binaries that have more crudely measured eccentricities, EB data are exquisite and have the power to constrain the process of tidal circularization. In the following, we briefly review a few previous works that have a relationship to our study here.

5.2. Other Previous Works

A number of recent studies have also noted the presence of eccentric binaries at short orbital periods. Studying field spectroscopic binaries (typically a few gigayears old) that are of order a few hundred in sample size, Triaud et al. (2017) found values of ∼7–9 days for the circularization period, in between that of ours ($P_{\rm circ} \sim 6$ days, Figure 5) and that of Meibom & Mathieu (2005) ($P_{\rm circ} \gtrsim 10$ days). Similarly, Price-Whelan et al. (2020) and Kounkel et al. (2021) also noticed that many binaries with very short orbital periods still have substantial eccentricities.[5] These studies conflict with Raghavan et al. (2010), who found a long circularization period of ∼12 days for solar-type field binaries, with few eccentric binaries below this period. However, the Raghavan et al. (2010) sample had ∼30 binaries with orbital periods less than 100 days, while the other aforementioned studies had >100 (Triaud et al. 2017; Price-Whelan et al. 2020).

Other studies have explored the eccentricity distributions of EBs, as discovered by Kepler and TESS, the very sample we adopt here (Van Eylen et al. 2016; Kjurkchieva et al. 2017; Justesen & Albrecht 2021). All noticed the significant presence of eccentric binaries within 10 days, in contradiction to a longer circularization period. Some of these studies have also investigated the dependency on stellar mass or effective temperature, reaching sometimes diverging results. For instance, while Torres et al. (2010), Van Eylen et al. (2016), and Justesen & Albrecht (2021) found that stars below the Kraft break (Kraft 1967) appear to be circularized out to longer periods, other works fail to find this trend (Kjurkchieva et al. 2017; Windemuth et al. 2019). We leave investigations on the eccentricity distribution of stars above and below the Kraft break to future works.

5.3. Implications for Theories of Tidal Dissipation

Our work reaches differing conclusions than Meibom & Mathieu (2005), whose constraints have guided theoretical studies of tidal dissipation in stars for close to two decades. We first discuss the relevance of the envelope period, where the most-eccentric binaries circularize interior to only ∼3 days, and later the distinct envelope and circularization periods of ∼3 and ∼6 days, for tidal theories.

5.3.1. The Envelope Period

At least the youngest binaries ($\lesssim$1 Gyr) circularize their orbits out to the envelope period, which has a value of ∼3 days for the eclipsing and spectroscopic binaries. This differs from the young binary circularization periods of ∼8 days reported by Meibom & Mathieu (2005) and has a bearing on numerous tidal theories.

A primary contender to the circularization of solar-like binaries is the dissipation of the equilibrium tide by convective turbulence (e.g., Zahn 1989). Zahn & Bouchet (1989) have estimated that binaries should be circularized out to ∼8 days after the pre-main sequence, rising slightly during the main sequence. This assumes that the equilibrium tide is efficiently

[5] Some of these may be fictitious; see Price-Whelan et al. (2020) for a discussion.

dissipated in the surface convection zones, with the magnitude of turbulent viscosity reduced in the fast-tide regime by a factor of $(P_{\rm orb}/\tau_{\rm cv})^{\xi}$ and $\xi = 1$. Here, $\tau_{\rm cv} \gg P_{\rm orb}$ is the characteristic convection turnover time. However, multiple works have instead advocated for a much steeper reduction of $\xi = 2$ for fast tides (Goldreich & Nicholson 1977; Goodman & Oh 1997). If so, the equilibrium tide can only circularize binaries out to ∼2 days during the pre-main sequence, and little beyond that during the main sequence (Goodman & Oh 1997; Goodman & Dickson 1998; Barker 2020; Zanazzi & Wu 2021). Recently, Terquem (2021) and Terquem & Martin (2021) have argued for the unsuppressed dissipation of tidal flows by turbulent convection, arguing that instead of the convective eddies serving as the turbulent viscosity for the tidal flow, the tidal flow works as a viscosity for the turbulent eddies. They find a circularization period of ∼6 days during the pre-main sequence, which increases by ∼1–2 days during the main sequence. The envelope period indirectly supports the most pessimistic estimates on the efficiency of convective damping (Goldreich & Nicholson 1977; Goodman & Dickson 1998), in agreement with recent hydrodynamical simulations (Ogilvie & Lesur 2012; Duguid et al. 2020a, 2020b; Vidal & Barker 2020a, 2020b; Barker & Astoul 2021).

Our results also have bearing on the character of dynamical tides. While dynamical tides without locking have been known to be ineffectual (e.g., Terquem et al. 1998), resonance locking can greatly prolong the duration of resonances between tidal forcing and stellar internal modes. This, as calculated by Zanazzi & Wu (2021), can circularize solar-type binaries out to ∼3–4 days over the first few million years (pre-main sequence). However, they found that resonance locking does not operate as efficiently during the main sequence, when the tidal resonances become too weak. The fact that $P_{\rm env} \sim 3$ days for the Kepler and TESS field binaries is consistent with resonance locking operating during the pre-main sequence.

Goodman & Dickson (1998), Ogilvie & Lin (2007), Barker & Ogilvie (2010), Barker & Ogilvie (2011), and Barker (2020) have pointed out the importance of nonlinear wave-breaking in enhancing the effectiveness of dynamical tides in main-sequence stars. As the radiative cores of these stars are strongly stratified, tidally excited gravity waves can grow in amplitude as they travel inward. If they overturn, they can deposit all their energy in the stellar core. Goodman & Dickson (1998) estimated that this can, over the main-sequence lifetime, circularize solar-type binaries out to ∼4–6 days. As this is only a modest increase of the envelope period ($P_{\rm env} \sim 3$ days), we could not confirm it using current EB data. We hope that the accumulation of a large sample of binaries, and reasonably precise main-sequence age-dating, will allow us to draw firm conclusions in the future.

5.3.2. Distinct Envelope and Circularization Periods

An important puzzle arises from our work: the presence of circular binaries out to ∼10–20 days, which we call the "cold core." We argue this feature dominates the determination of $P_{\rm circ} \sim 6$ days for the Kepler/TESS EBs. This overdensity of circular binaries may be a feature of binary formation, implying $P_{\rm env}$ is the only "true" measure of tidal circularization. It has been argued that solar-type close binaries (inward of 10 au) are likely the result of disk fragmentation (see, e.g., Kratter et al. 2010; Kuruwita & Federrath 2019; Moe et al. 2019; Kuruwita et al. 2020; Tokovinin & Moe 2020), hence these binaries would be subject to eccentricity damping from their nascent disks. On the other hand, such a scenario fails to explain why many close binaries remain eccentric (to subsequently be tidally circularized). It also cannot explain why binaries hosting circumbinary disks are often eccentric (e.g., Czekala et al. 2019).

The cold core could also have a primordial tidal origin, but this requires a mechanism that selectively circularizes only a subset of solar-type binaries. One possibility is circularization via inertial-wave dissipation. The diversity of pre-main-sequence rotation periods (e.g., Bouvier 2013) would allow inertial waves to selectively synchronize and then circularize stars born with rapid rotation rates. Recent calculations by Barker (2022) support this hypothesis and show inertial waves may indeed be able to circularize synchronous binaries out to ∼10 day orbital periods.

If the eccentricity envelope and cold core are the results of age-dependent circularization, the tidal dissipation mechanism cannot depend strongly on the binary separation. Letting $t_{\rm young}$ ($t_{\rm old}$) be the ages, and $P_{\rm young}$ ($P_{\rm old}$) the circularization period, of the young (old) binaries, Equation (3) gives

$$\frac{t_{\rm young}}{t_{\rm old}} = \left(\frac{P_{\rm young}}{P_{\rm old}}\right)^{\eta}. \tag{4}$$

The Kepler and TESS EB data requires $\eta \lesssim 2.4$ to explain the two circularization periods ($P_{\rm young} \lesssim P_{\rm env}$, $P_{\rm old} \gtrsim P_{\rm circ}$), assuming $t_{\rm young} \approx 1$ Gyr and $t_{\rm old} \approx 5$ Gyr. Table 1 lists η values for different tidal theories: All have η values significantly larger than 2.4. Thus, although no existing tidal theory can give rise to the two circularization periods, a tidal origin cannot be excluded.

Table 1
Tidal Theory Values for η (Equation (3))

Tidal Theory	η
Convection Zone Damping[1,2,3,4,5]	3.33–6.05
Nonresonant Radiative Diffusion[1,4]	7
Nonresonant Inertial Waves[6,4]	6.33
Nonlinear Wave-breaking[7,8]	7

Note. We require $\eta \lesssim 2.4$ to explain the circularization and envelope periods in the Kepler/TESS data, not predicted by any tidal theory. References: (1) Zahn (1977), (2) Goldreich & Nicholson (1977), (3) Goodman & Oh (1997), (4) Barker (2020), (5) Terquem (2021), (6) Ogilvie & Lin (2007), (7) Goodman & Dickson (1998), (8) Barker & Ogilvie (2010).

6. Conclusions

In this work, we employ ∼500 EBs discovered by the Kepler and TESS missions to constrain the process of tidal dissipation. With exquisite measurements of the eccentricities (encompassing a dynamic range of $\sim 10^3$), EBs are unique and powerful tools for this goal.

We introduce the so-called envelope period to quantify where only the most-eccentric binaries circularize and calculate its value to be ∼3 days, much shorter than the circularization period we find of ∼6 days. The circularization period is strongly affected by the presence of many nearly circular binaries out to ∼10–20 day orbital periods (the "cold core"). We posit three scenarios to generate an envelope period much shorter than the circularization period: primordial formation of the "cold core" by disk migration and damping, selective circularization via inertial

waves, and age-dependent circularization of field binaries. These findings are in direct tension with results reported by Meibom & Mathieu (2005), who studied spectroscopic binaries collected from various open clusters. We point out that the presence of the "cold core" population, together with a much smaller sample size per cluster, may have explained much of the discrepancies between our results and theirs. However, we reaffirm that their data do show a significant difference between the eccentricity distributions of young (<1 Gyr) and old (>3 Gyr) binaries. More data are needed for a stronger conclusion. Of particular benefit would be many more binaries from the pre-main-sequence phase, such as those collected by Melo et al. (2001) and Ismailov et al. (2014), and accurate age constraints for field stars.

Our results, if confirmed, have the potential to reconcile tidal theories with observations. Assuming the fast-tide reduction supported by recent hydrodynamical simulations, equilibrium tides are not expected to play a significant role in both the main sequence and the pre-main sequence.[6] First-principles calculations of resonance locking find solar-type binaries circularize out to $\sim$3 days before they arrive at the main sequence. Circularization by resonance locking is consistent with the envelope period introduced in this work. We cannot, at the moment, exclude a modest rise of the circularization period during the main sequence, as predicted by theories of wave-breaking. More EBs with well-defined ages will be needed to answer this.

Lastly, while our study sheds light on the circularization of solar-type binaries, there remains much beyond. For instance, stars with radiative envelopes may experience different tidal physics (e.g., Zahn 1975; Savonije & Papaloizou 1983; Goldreich & Nicholson 1989; Su & Lai 2021). EB data from OGLE and other surveys may provide useful constraints (Wyrzykowski et al. 2003; Pawlak et al. 2016, for LMC and SMC).

I dedicate this paper to Dr. Jing Lou, a bright and caring astrophysicist who passed away far too soon on 2022 February 15. Rest in peace Space Cowboy. I thank Yanqin Wu for the significant effort she put into this project, in both the analysis and interpretation of the data. I thank the referee, Robert Mathieu, for his constructive feedback, which significantly improved the quality of this work, and clarity of the manuscript. I also thank Simon Albrecht, Katie Breivik, Nathan Hara, Juna Kollmeier, Maxwell Moe, Norman Murray, Adrian Price-Whelan, Scott Tremaine, Amaury Triaud, Joshua Winn, and Wei Zhu for helpful conversations. J.Z. was supported by the Natural Sciences and Engineering Research Council of Canada (NSERC) under the funding reference # CITA 490888-16.

Appendix A
Eccentricity Vectors

Here, we briefly review how the eccentricities of EBs are measured (see Winn 2010 for a pedagogical review) and justify our procedure of using one component of the eccentricity vector to constrain tidal evolution.

Consider an EB with the primary and secondary eclipses occurring at time t_p and t_s, lasting a duration T_p and T_s, respectively. Let the pericenter angle relative to the line of sight be ω. We have

$$t_s - t_p \simeq \frac{P_{\rm orb}}{2}\left(1 + \frac{4}{\pi} e\cos\omega\right), \tag{A1}$$

$$\frac{T_s}{T_p} \simeq \frac{1 + e\sin\omega}{1 - e\sin\omega}, \tag{A2}$$

when $e \ll 1$. These allow both the $e\cos\omega$ and $e\sin\omega$ components to be measured from the lightcurve.

However, while the transit centroids (t_s, t_p) can be accurately determined (with similar precision as for the orbital period), the measurements of T_s and T_p are much less precise—they depend on factors like limb darkening, observational cadence, and stellar noise (e.g., Van Eylen et al. 2016; Windemuth et al. 2019; Justesen & Albrecht 2021). As a result, the values of $e\cos\omega$ are typically known much better than those of $e\sin\omega$. This explains the strange clustering seen in Figure 2. In order to utilize the full potential of EB data, we have therefore opted to focus only on the $e\cos\omega$ measurements.

Appendix B
Synthetic Observations of Circularized Binaries

To understand how the sample size impacts measurements of the circularization and envelope period, we produce synthetic observations of tidally circularized binaries. Given an initial binary eccentricity e and orbital period $P_{\rm orb}$, we assume pseudo-synchronous rotation and evolve the binary orbit as (Hut 1981)

$$\frac{1}{e}\frac{{\rm d}e}{{\rm d}t} = \frac{\mu(1+\mu)}{t_c} F_e(e), \tag{B1}$$

$$\frac{1}{P_{\rm orb}}\frac{{\rm d}P_{\rm orb}}{{\rm d}t} = \frac{3\mu(1+\mu)}{2t_c} F_a(e), \tag{B2}$$

where $\mu \leqslant 1$ is the mass ratio,

$$F_e(e) = \frac{\Omega_e(e)N(e)}{\Omega(e)} - \frac{18}{11}N_e(e), \tag{B3}$$

$$F_a(e) = \frac{4}{11}\left[\frac{N^2(e)}{\Omega(e)} - N_a(e)\right], \tag{B4}$$

and the functions $N(e)$, $\Omega(e)$, $\Omega_e(e)$, $N_a(e)$, and $N_e(e)$ are defined in Leconte et al. (2010). We parameterize the circularization period as

$$t_c = 0.3\ {\rm Gyr}\left(\frac{P_{\rm orb}}{4\ {\rm day}}\right)^{\eta}, \tag{B5}$$

with η a free parameter that governs how strongly t_c depends on the binary separation (see Table 1 for physical η values).

Our initial distribution of e, $P_{\rm orb}$, and μ values are motivated by observations. We draw eccentricity values from a beta distribution $\mathcal{B}(e|a, b)$, with $a = 1.75$ and $b = 2.01$, constrained from the APOGEE Gold Sample (Price-Whelan et al. 2020). We take the eccentricity distribution of intermediate-period binaries for simplicity because a short-period distribution must take into account formation and tidal evolution simultaneously (e.g., Fabrycky & Tremaine 2007; Moe & Kratter 2018; Tokovinin & Moe 2020). Mass ratios are drawn from a linear distribution $\mathcal{P}(\mu) \propto \mu$ to mimic the abundance of equal-mass binaries at short periods (e.g., Raghavan et al. 2010;

[6] We note that dissipation of red giant binaries is well explained by turbulent damping of the equilibrium tide Verbunt & Phinney (1995) and Price-Whelan & Goodman (2018). However, these are not in the "fast-tide" limit.

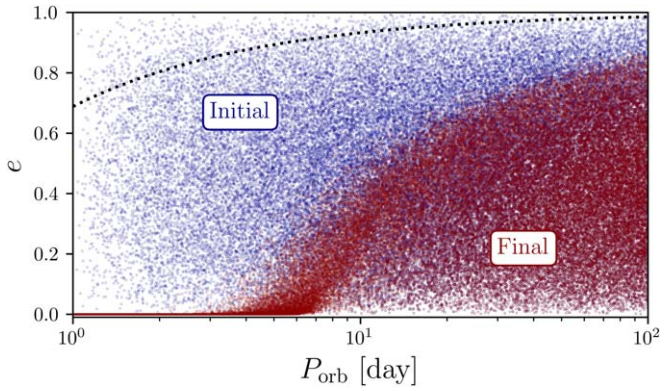

Figure 7. Initial (blue) and final (red) population of binaries after tidal circularization, for $\eta = 4.5$. Black dotted line displays the periastron distance of $r_{\rm p} = 1.5\ R_\odot$. See text for details.

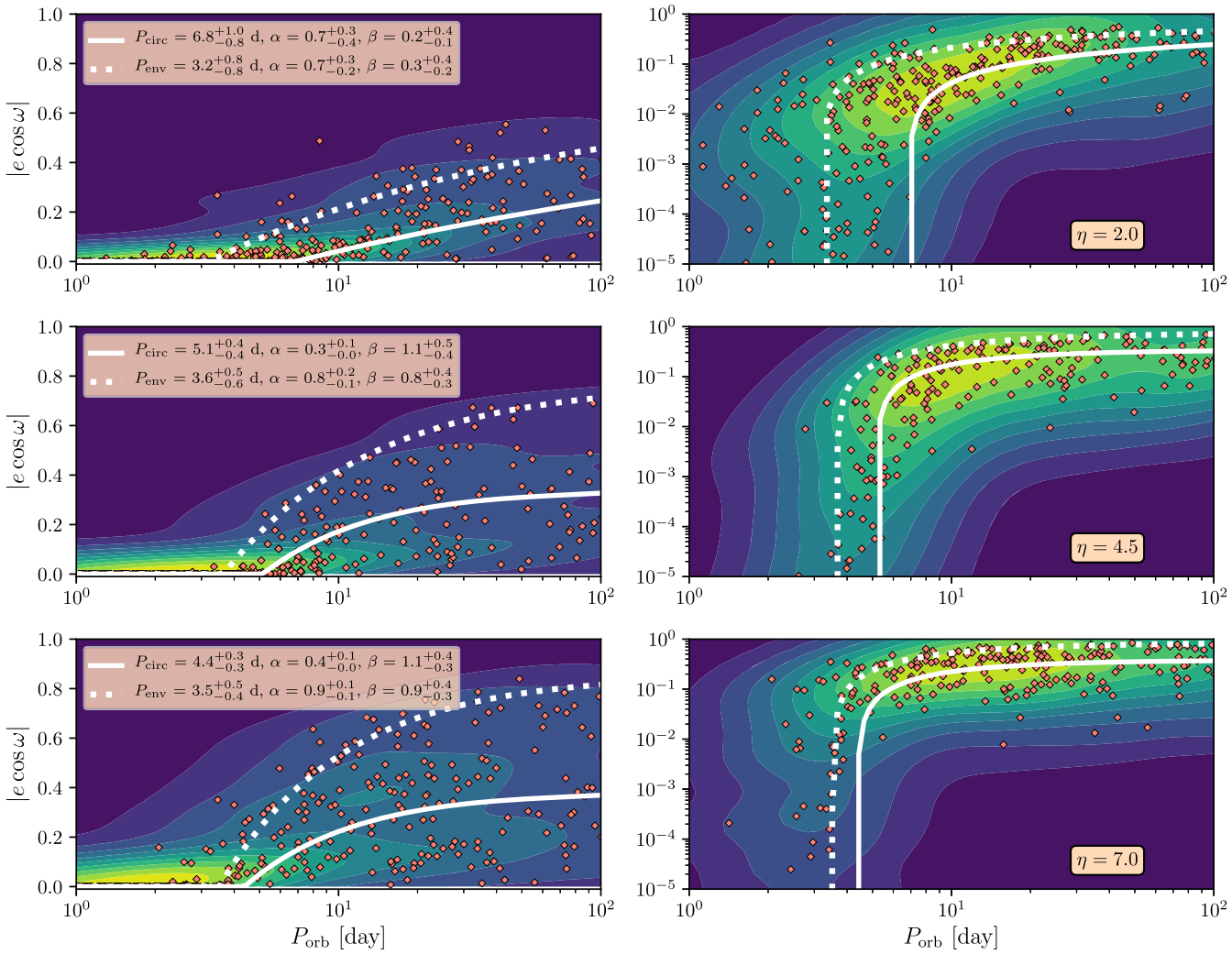

Figure 8. Synthetic observations of $N_b = 524$ tidally circularized binaries, for the η values indicated. Salmon diamonds denote projected eccentricity measurements, contours denote smoothed kernel density estimates of the projected eccentricities, while solid (dotted) lines denote $P_{\rm circ}$ ($P_{\rm env}$) fits to 1000 observations of the circularized population. The $P_{\rm circ}$, $P_{\rm env}$ parameter fits are displayed in the legends.

Moe & Di Stefano 2017; Windemuth et al. 2019). To approximate the binary-period log-normal distribution centered at $P_{\rm orb} \sim 250$ yr (Raghavan et al. 2010), we assign initial periods through

$$\ln P_{\rm orb} = (1 - \lambda)\ln P_{\rm min} + \lambda \ln P_{\rm max}, \tag{B6}$$

with $0 \leqslant \lambda \leqslant 1$ drawn from a linear distribution $\mathcal{P}(\lambda) \propto \lambda$, with $P_{\rm min} = 1$ day and $P_{\rm max} = 200$ days. We integrate Equations (B1)–(B2) for $N_{\rm tot} = 10^5$ binaries from $t = 0$ to the binary age $t = t_{\rm age}$, uniformly distributed between 1 and 10 Gyr. Figure 7 displays the initial and final population for one of our

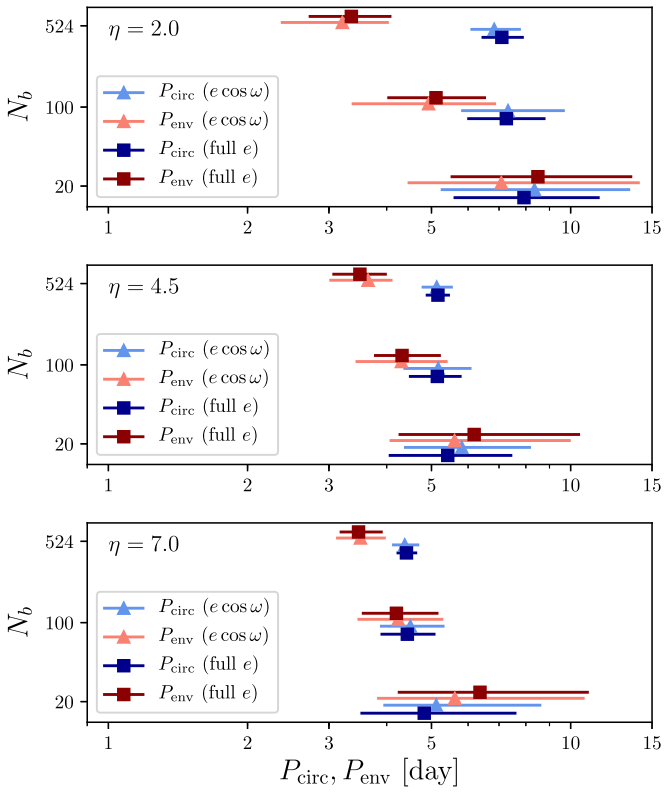

Figure 9. Comparing $P_{\rm circ}$, $P_{\rm env}$ constraints using the projected (triangles) and full (squares) eccentricity measurements, drawing N_b binaries from the tidally circularized population, for the η values indicated. Lines denote 1σ errors, slightly displaced from their y-axis N_b value for clarity. There is no notable difference between $P_{\rm circ}$, $P_{\rm env}$ constraints using the projected versus full eccentricity measurements.

simulations. We see a negligible amount of binaries in our initial distribution collide (periastron distances shorter than 1.5 $R_\odot$; Raghavan et al. 2010).

To generate a synthetic observation, we assign each binary a longitude of pericenter ω, distributed uniformly between 0 and 2π. Projected eccentricities $|e\cos\omega|$ are measured by drawing N_b binaries from the theoretical population, weighted by the probability primary and secondary eclipses are observed (e.g., Winn 2010):

$$p_{\rm ecl} \propto \frac{1}{a}\left(\frac{1-|e\sin\omega|}{1-e^2}\right). \tag{B7}$$

We calculate $P_{\rm circ}$ and $P_{\rm env}$ for the N_b EBs and repeat this process $N_s = 10^3$ times.

Our simulations find a stronger dependence of eccentricity damping on the orbital period leads to a more narrow range of circularization periods. Figure 8 displays synthetic observations of our simulations, alongside constraints on the circularization period. We see only low values of η can lead to significantly different circularization periods. We also see tidal dissipation can lead to a wide range of very small eccentricity values at short orbital periods, seen also in the EB data (the "waterfall" in Figure 4).

However, a natural question is if the circularization period constraint differs if one only uses the projected eccentricities from EBs or the full eccentricities from spectroscopic binaries. To check if keeping only the projected eccentricities alters the determination of $P_{\rm circ}$ or $P_{\rm env}$, we compare our EB $P_{\rm env}$ and $P_{\rm circ}$ values to synthetic spectroscopic binary values. To create an observation of spectroscopic binaries, the orbits of N_b binaries are drawn randomly from our simulation, and then Equation (1) is fit to the full eccentricity and orbital period data. Figure 9 displays the results of this calculation, where we find no significant difference in $P_{\rm env}$ and $P_{\rm circ}$ values when fit to eclipsing or spectroscopic binaries.

ORCID iDs

J. J. Zanazzi https://orcid.org/0000-0002-9849-5886

References

Barker, A. J. 2020, MNRAS, 498, 2270
Barker, A. J. 2022, ApJL, 927, L36
Barker, A. J., & Astoul, A. A. V. 2021, MNRAS, 506, L69
Barker, A. J., & Ogilvie, G. I. 2010, MNRAS, 404, 1849
Barker, A. J., & Ogilvie, G. I. 2011, MNRAS, 417, 745
Borucki, W. J., Koch, D., Basri, G., et al. 2010, Sci, 327, 977
Bouvier, J. 2013, in Role and Mechanisms of Angular Momentum Transport During the Formation and Early Evolution of Stars, EAS Publication Series, 62, ed. P. Hennebelle & C. Charbonnel (Les Ulis: EDP Sciences), 143
Burkart, J., Quataert, E., Arras, P., & Weinberg, N. N. 2012, MNRAS, 421, 983
Czekala, I., Chiang, E., Andrews, S. M., et al. 2019, ApJ, 883, 22
Duguid, C. D., Barker, A. J., & Jones, C. A. 2020a, MNRAS, 497, 3400
Duguid, C. D., Barker, A. J., & Jones, C. A. 2020b, MNRAS, 491, 923
Fabrycky, D., & Tremaine, S. 2007, ApJ, 669, 1298
Fuller, J. 2017, MNRAS, 472, 1538
Fuller, J., & Lai, D. 2012, MNRAS, 420, 3126
Geller, A. M., Hurley, J. R., & Mathieu, R. D. 2013, AJ, 145, 8
Geller, A. M., & Mathieu, R. D. 2012, AJ, 144, 54
Geller, A. M., Mathieu, R. D., Latham, D. W., et al. 2021, AJ, 161, 190
Goldreich, P., & Nicholson, P. D. 1977, Icar, 30, 301
Goldreich, P., & Nicholson, P. D. 1989, ApJ, 342, 1079
Goodman, J., & Dickson, E. S. 1998, ApJ, 507, 938
Goodman, J., & Lackner, C. 2009, ApJ, 696, 2054
Goodman, J., & Oh, S. P. 1997, ApJ, 486, 403
Hamers, A. S. 2019, MNRAS, 482, 2262
Hut, P. 1981, A&A, 99, 126
Ismailov, N. Z., Abdi, H. A., & Mamedxanova, G. B. 2014, ATsir, 1610, 1
Justesen, A. B., & Albrecht, S. 2021, ApJ, 912, 123
Kirk, B., Conroy, K., Prša, A., et al. 2016, AJ, 151, 68
Kjurkchieva, D., Vasileva, D., & Atanasova, T. 2017, AJ, 154, 105
Kounkel, M., Covey, K. R., Stassun, K. G., et al. 2021, AJ, 162, 184
Kraft, R. P. 1967, ApJ, 150, 551
Kratter, K. M., Matzner, C. D., Krumholz, M. R., & Klein, R. I. 2010, ApJ, 708, 1585
Kuruwita, R. L., & Federrath, C. 2019, MNRAS, 486, 3647
Kuruwita, R. L., Federrath, C., & Haugbølle, T. 2020, A&A, 641, A59
Latham, D. W., Mathieu, R. D., Milone, A. A. E., & Davis, R. J. 1992, in ASP Conf. Ser. 32, IAU Colloq. 135: Complementary Approaches to Double and Multiple Star Research, ed. H. A. McAlister & W. I. Hartkopf (San Francisco, CA: ASP), 152
Leconte, J., Chabrier, G., Baraffe, I., & Levrard, B. 2010, A&A, 516, A64
Leiner, E. M., Mathieu, R. D., Gosnell, N. M., & Geller, A. M. 2015, AJ, 150, 10
Lin, Y., & Ogilvie, G. I. 2018, MNRAS, 474, 1644
Lin, Y., & Ogilvie, G. I. 2021, ApJL, 918, L21
Ma, L., & Fuller, J. 2021, ApJ, 918, 16
Mathieu, R. D., & Mazeh, T. 1988, ApJ, 326, 256
Mathieu, R. D., Meibom, S., & Dolan, C. J. 2004, ApJL, 602, L121
Mayor, M., & Mermilliod, J. C. 1984, in Observational Tests of the Stellar Evolution Theory. International Astronomical Union Symposium No. 105, ed. A. Maeder & A. Renzini (Dordrecht: Reidel), 411
Mazeh, T. 2008, in EAS Publications Series, 29, ed. M. J. Goupil & J. P. Zahn (Les Ulis: EDP Sciences), 1
Mazeh, T., & Shaham, J. 1978, A&A, 77, 145
Meibom, S., & Mathieu, R. D. 2005, ApJ, 620, 970
Meibom, S., Mathieu, R. D., & Stassun, K. G. 2006, ApJ, 653, 621
Melo, C. H. F., Covino, E., Alcalá, J. M., & Torres, G. 2001, A&A, 378, 898
Milliman, K. E., Mathieu, R. D., Geller, A. M., et al. 2014, AJ, 148, 38
Moe, M., & Di Stefano, R. 2017, ApJS, 230, 15
Moe, M., & Kratter, K. M. 2018, ApJ, 854, 44

Moe, M., Kratter, K. M., & Badenes, C. 2019, ApJ, 875, 61
Morbidelli, A., Levison, H. F., & Gomes, R. 2008, in The Solar System Beyond Neptune, ed. M. A. Barucci et al. (Tucson, AZ: Univ. of Arizona Press), 275
Naoz, S., & Fabrycky, D. C. 2014, ApJ, 793, 137
Nine, A. C., Milliman, K. E., Mathieu, R. D., et al. 2020, AJ, 160, 169
North, P., & Zahn, J. P. 2003, A&A, 405, 677
Ogilvie, G. I., & Lesur, G. 2012, MNRAS, 422, 1975
Ogilvie, G. I., & Lin, D. N. C. 2007, ApJ, 661, 1180
Pawlak, M., Soszyński, I., Udalski, A., et al. 2016, AcA, 66, 421
Penev, K., Sasselov, D., Robinson, F., & Demarque, P. 2007, ApJ, 655, 1166
Price-Whelan, A. M., & Goodman, J. 2018, ApJ, 867, 5
Price-Whelan, A. M., Hogg, D. W., Foreman-Mackey, D., & Rix, H.-W. 2017, ApJ, 837, 20
Price-Whelan, A. M., Hogg, D. W., Rix, H.-W., et al. 2020, ApJ, 895, 2
Prša, A., Batalha, N., Slawson, R. W., et al. 2011, AJ, 141, 83
Raghavan, D., McAlister, H. A., Henry, T. J., et al. 2010, ApJS, 190, 1
Ricker, G. R., Winn, J. N., Vanderspek, R., et al. 2015, JATIS, 1, 014003
Savonije, G. J., & Papaloizou, J. C. B. 1983, MNRAS, 203, 581
Savonije, G. J., & Papaloizou, J. C. B. 1984, MNRAS, 207, 685
Savonije, G. J., & Witte, M. G. 2002, A&A, 386, 211
Slawson, R. W., Prša, A., Welsh, W. F., et al. 2011, AJ, 142, 160
Su, Y., & Lai, D. 2022, MNRAS, 510, 4943
Terquem, C. 2021, MNRAS, 503, 5789
Terquem, C., & Martin, S. 2021, MNRAS, 507, 4165
Terquem, C., Papaloizou, J. C. B., Nelson, R. P., & Lin, D. N. C. 1998, ApJ, 502, 788
Tokovinin, A., & Moe, M. 2020, MNRAS, 491, 5158
Torres, G., Andersen, J., & Giménez, A. 2010, A&ARv, 18, 67
Triaud, A. H. M. J., Martin, D. V., Ségransan, D., et al. 2017, A&A, 608, A129
Van Eylen, V., Winn, J. N., & Albrecht, S. 2016, ApJ, 824, 15
Verbunt, F., & Phinney, E. S. 1995, A&A, 296, 709
Vidal, J., & Barker, A. J. 2020a, MNRAS, 497, 4472
Vidal, J., & Barker, A. J. 2020b, ApJL, 888, L31
Windemuth, D., Agol, E., Ali, A., & Kiefer, F. 2019, MNRAS, 489, 1644
Winn, J. N. 2010, in Exoplanet Transits and Occultations, ed. S. Seager (Tucson, AZ: Univ. of Arizona Press), 55
Witte, M. G., & Savonije, G. J. 1999, A&A, 350, 129
Witte, M. G., & Savonije, G. J. 2001, A&A, 366, 840
Witte, M. G., & Savonije, G. J. 2002, A&A, 386, 222
Wu, Y. 2005, ApJ, 635, 688
Wyrzykowski, L., Udalski, A., Kubiak, M., et al. 2003, AcA, 53, 1
Zahn, J. P. 1966, AnAp, 29, 489
Zahn, J. P. 1975, A&A, 41, 329
Zahn, J. P. 1977, A&A, 500, 121
Zahn, J. P. 1989, A&A, 220, 112
Zahn, J. P., & Bouchet, L. 1989, A&A, 223, 112
Zanazzi, J. J., & Wu, Y. 2021, AJ, 161, 263